Eur. Phys. J. Plus (2021) 136:690
https://doi.org/10.1140/epjp/s13360-021-01681-9

THE EUROPEAN PHYSICAL JOURNAL PLUS

Regular Article

Cylindrical neutron spectrometer system: design and characterization

Ngoc-Thiem Le[1,a], Ngoc-Quynh Nguyen[1], Huu-Quyet Nguyen[1], Duc-Khue Pham[1], Minh-Cong Nguyen[2], Van-Loat Bui[3], Van-Chung Cao[4], Van-Hao Duong[5], Trung H. Duong[6], Hoai-Nam Tran[7,8,b]

[1] Institute for Nuclear Science and Technology, VINATOM, 179 Hoang Quoc Viet, Hanoi 100000, Viet Nam
[2] Military Institute for Chemistry and Environment, An Khanh, Hoai Duc, Hanoi 100000, Viet Nam
[3] Faculty of Physics, VNU University of Science, 334 Nguyen Trai, Hanoi 100000, Viet Nam
[4] Research and Development Center for Radiation Technology, VINATOM, Thu Duc, Ho Chi Minh city 700000, Viet Nam
[5] Hanoi University of Mining and Geology, Hanoi 100000, Viet Nam
[6] Department of Engineering, Colorado State University-Pueblo, Pueblo, CO, USA
[7] Institute of Fundamental and Applied Sciences, Duy Tan University, Ho Chi Minh city 700000, Viet Nam
[8] Faculty of Natural Sciences, Duy Tan University, Da Nang 550000, Viet Nam

Received: 14 January 2021 / Accepted: 17 June 2021

Abstract A multilayer cylindrical neutron spectrometer (CNS) system has been designed based on the similar principle of a commercial Bonner sphere spectrometer (BSS) system. The characteristics, e.g., spectral neutron fluence response functions and angular neutron fluence response functions, of the CNS system have been evaluated using MCNP6 simulations. The dosimetric quantities including neutron fluence rate (φ_E), neutron ambient dose equivalent rate ($\dot{H}^*(10)$), neutron ambient dose equivalent-averaged energy ($\widetilde{E}$), neutron fluence-averaged energy ($\overline{E}$) and neutron fluence-to-ambient dose equivalent conversion coefficient ($\overline{h}_\phi$) of three neutron standard fields with ^{241}Am–Be source were evaluated using the CNS system. The standard uncertainties of the dosimetric quantities were also estimated and discussed. Comparison of dosimetric quantities measured by the CNS and the BSS systems was made in order to verify the operation of the CNS system. The discrepancies in φ_E, $\dot{H}^*(10)$, $\widetilde{E}$, $\overline{E}$ and $\overline{h}_\phi$ measured by the CNS and the BSS systems are 7%, 5%, 8%, 11% and 3%, respectively. This agreement indicates that the CNS system is reliable for neutron dosimetry and radiation safety assessment. The CNS system is advantageous due to its compactness, portability and simplicity in fabrication.

1 Introduction

Precise measurement of the intrinsic characteristics of neutrons as neutral particles with continuous fluence rate spectra is still a challenge in spectrometry and dosimetry aspects. Bonner Sphere Spectrometer (BSS) system has been emerged as an useful and effective

[a] e-mail: LNThiem@vinatom.gov.vn (corresponding author)
[b] e-mail: tranhoainam4@dtu.edu.vn (corresponding author)

Published online: 25 June 2021

instrument for neutron spectrometry and dosimetry [1,2]. Radiation Protection Laboratory (RPL) of the Institute for Nuclear Science and Technology (INST) (Hanoi, Vietnam) has been equipped with a BSS system, which consists of a Ludlum 2200 scaler electrometer and six polyethylene (PE) spheres with the diameters of 2, 3, 5, 8, 10 and 12 inches [3–6]. The BSS system consists of a ^{6}LiI(Eu) cylindrical thermal neutron scintillator detector (4.0 mm in diameter and 4.0 mm in height, model 42-5 of the Ludlum Measurements Inc.) sitting at the center of the high density (ρ = 0.95 g/cm^3) PE spherical moderators. Several neutron standard fields have been established at RPL–INST and characterized using the BSS system such as a neutron calibration field of a bare ^{252}Cf source [3], a neutron calibration field of a bare ^{241}Am–Be source [4] and simulated workplace neutron fields of ^{241}Am–Be sources moderated by PE spheres [5].

For the purpose of neutron dosimetry and safety assessment at various radiation facilities, it is desirable to develop a cylindrical neutron spectrometer (CNS) which is more compact and portable when taking into account the convenience for transportation in the practical usage. Particularly, in the CNS system, a smaller cylindrical moderator can be put into a bigger one, and therefore, the volume and the total weight of the combined system could be significantly reduced in comparison with that of the BSS system. Many attempts have been performed to fabricate neutron spectrometers' moderators with different shapes: (i) a CNS system using a single active ^{3}He thermal neutron detector at the center of multiple cylindrical PE moderators to measure neutron spectrum from a ^{252}Cf source [7], or in radiotherapy bunkers [8]; (ii) three kinds of neutron spectrometers with cylindrical, spherical and rotational moderators were used to measure neutron spectra around research nuclear reactors [9]; (iii) the CNS system with a ^{6}LiI(Eu) thermal neutron scintillator was fabricated and characterized in the neutron standard field of an ^{241}Am–Be source [10,11]; (iv) a proposed gold-and-indium dual activation foil-based BSS was characterized in neutron standard fields of ^{252}Cf and ^{241}Am–Be sources [12]; (v) the BSS system with different thermal neutron detectors were applied to investigate neutron spectra in pulsed fields [13], at high altitude background neutron spectra [14], in the fields of neutron radioisotopes [15,16], or at workplaces [17]; and (vi) multiple active thermal neutron detectors located in a single moderator were used to monitor neutrons at workplaces [18,19].

In the present work, a CNS system consisting of a ^{6}LiI(Eu) cylindrical thermal neutron scintillator detector and multilayer cylindrical moderators has been proposed and designed based on the similar principle of the commercial BSS system [1]. The angular neutron fluence responses and spectral neutron fluence response functions of the CNS system were calculated for each combination of the ^{6}LiI(Eu) thermal neutron detector and a cylindrical moderator based on Monte Carlo simulations using the MCNP6 code [20]. To calibrate and verify the performance of the designed CNS system, the CNS system has been used to characterize the dosimetric quantities due to the total component of the neutron fields, i.e., neutron fluence rate, φ_E; neutron ambient dose equivalent rate, $\dot{H}^*(10)$; neutron ambient dose equivalent-averaged energy, $\widetilde{E}$; neutron fluence-averaged energy, $\overline{E}$; and neutron fluence-to-ambient dose equivalent conversion coefficient, $\overline{h}_\phi$, of several ^{241}Am–Be neutron standard fields in comparison with that obtained using a well-calibrated BSS system [4,5].

2 Materials and methods

2.1 Neutron standard fields

A neutron calibration room at the RPL–INST has the inner dimensions of 700 cm × 700 cm × 700 cm, constructed of ordinary concrete with the density of 2.35 g/cm^{-3} approximate the NBS-03 type concrete reported by the Pacific Northwest National Laboratory [21]. It was equipped with a ^{241}Am–Be source (X14 type capsulation, supplied by the Hopewell Designs, Inc., USA). The source was installed in a container at the floor center with the neutron emission rate of $1.299 \times 10^7\ s^{-1}$ on 23 January 2015 with the expanded uncertainty of 2.9% (a coverage factor of 2 or k=2 with a confidence level of 95%). Based on the ^{241}Am–Be source, several neutron standard fields have been established by using the bare source [4] and/or moderated sources [5]. In the present work, experiments have been performed with the CNS system in three neutron standard fields: (i) a neutron standard field of the bare ^{241}Am–Be source and (ii) two simulated workplace neutron standard fields of the ^{241}Am–Be source moderated by high density PE spheres with diameters of 20 cm (denoted as 20PE(^{241}Am–Be)) and 30 cm (denoted as 30PE(^{241}Am–Be)), respectively. The above-mentioned dosimetric quantities of the three neutron standard fields have been characterized using the BSS system in previous works [4,5,22], which are used as the reference data to quantify the CNS measurement in order to confirm the reliability of the CNS system.

In general, a neutron spectrometer or dosimeter consists of a single thermal neutron detector and multiple neutron moderators, e.g., the BSS system [1,7,9], or multiple thermal neutron detectors and single/multiple neutron moderator/s [12–19,23,24]. Among several neutron spectrometers and dosimeters, the BSS system is one of the most common and effective devices which has been used widely in many dosimetry laboratories. The RPL–INST–BSS system configuration allows detecting neutrons from thermal energy up to 20 MeV and is not sensitive to gammas. The thermal neutrons are detected by reactions ^{6}Li$(n, \alpha)^3H$ (Q = 4.78 MeV); then, the Ludlum 2200 scaler counts the electronic pulses from a photomultiplier. More detailed description of the BSS system can be found in Ref. [1,4,5].

2.2 Cylindrical neutron spectrometer

Based on the similar principle of the BSS system, a CNS system has been designed to improve the compactness and portability for the practical usage at various radiation facilities. The same ^{6}LiI(Eu) cylindrical thermal neutron scintillator detector of the BSS system (with 96% ^{6}Li) was used in the CNS system. In addition, six cylindrical moderators with different dimensions were constructed accompanying with the ^{6}LiI(Eu) detector to combine the CNS system. The cylindrical moderators were designed so that a smaller cylinder can be put into a bigger one. The moderators were made of PE ($\rho = 0.95\ g/cm^3$), and the quality of PE material was controlled during fabrication. The densities of the PE cylinders were also re-evaluated based on the weights (measured by a standard balance at the Vietnam Metrology Institute) and the volumes (determined from their geometries). Figure 1 shows the CNS system (upper photo) and an internal view of the neutron standard room (lower photo).

In order to determine the optimal dimensions, i.e., the diameter and the height of the cylindrical moderators, the diameters of the six cylindrical moderators were firstly selected as 2, 3, 5, 8, 10 and 12 inches, respectively (which were the same as that of the BSS system). Then the heights of the cylindrical moderators were determined based on Monte Carlo simulations using the MCNP6 code [20]. The MCNP6 simulations were performed to evaluate the neutron fluence responses of the CNS system as functions of neutron incident angles from 0^o to 90^o

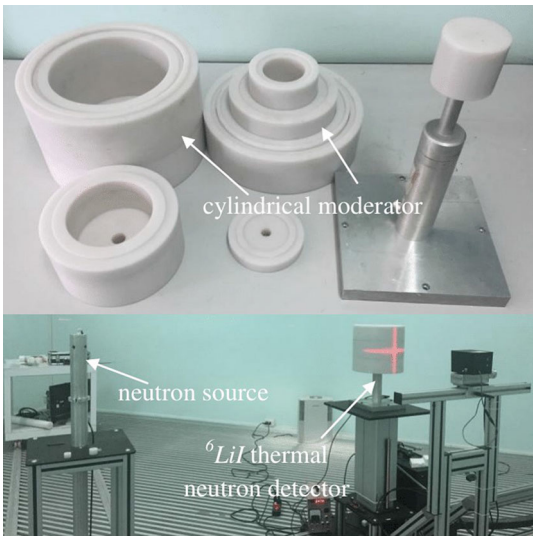

Fig. 1 Cylindrical neutron spectrometer system consisting of a ^{6}LiI thermal neutron detector and six cylindrical polyethylene moderators (upper), and an internal view of the neutron calibration room (lower)

with a step of 15^{o}. The angles of 0^{o} and 90^{o} correspond to the neutrons coming along and perpendicular to the central axis of the cylindrical moderators, respectively. The geometries are selected for manufacturing when the neutron fluence response ratios between other angles and the angle of 90^{o} approach to unity, i.e., the CNS system responses are close to isotropic. In this investigation, it is found that the optimal responses were obtained when the height-to-diameter ratios of the cylindrical moderators were chosen as 0.9. Table 1 presents the selected dimensions and the simulated relative neutron fluence responses of the CNS system. In the MCNP6 simulations, the number of particle histories greater than 2×10^{9} were chosen to ensure the statistical uncertainties of the fluence responses within $\pm 1\%$. The relative neutron fluence responses were normalized to the response of the bare detector in the neutron standard field with a bare ^{241}Am–Be source. Figure 2 displays the simulated angular neutron fluence responses of the CNS system with the normalization of the responses to that at the angle of 90^{o}. The angular neutron fluence responses vary due to the incident angles of neutrons, i.e., increasing/decreasing with the decrease/increase of the integrated trajectories of neutrons to reach the thermal neutron detector at that angle. The normalized angular neutron fluence responses tend to be close to that at 90^{o} when the neutron incident angle reached by 20^{o}. From Fig. 2, one can see that the CNS system has good angular responses because the neutron fluence responses at most of the angles are obtained with the discrepancies less than $\pm 3\%$ compared to that at 90^{0}. The largest discrepancy is less than 8% for the CNS-12 at 45^{o}. This difference is satisfied the IEC 61005 criteria on the variation of the response due to angles of incident neutrons (acceptable within 25%) [25].

2.3 Fluence response functions of the CNS system

Before putting the CNS system in the practical usage, the fluence responses as functions of neutron incident energies of the CNS system have been evaluated based on Monte Carlo simulations using the MCNP6 code. To ensure the accuracy of the response functions of the CNS system, the MCNP6 simulations were firstly performed to evaluate the BSS system's neutron fluence responses as functions of neutron incident energies and then compared to the data published in the IAEA compendium [26]. Comparisons between the simulated BSS

Table 1 Summary of the geometries and the simulated relative neutron fluence responses of the CNS moderators

CNS moderator name	Diameter (inch)	Height (inch)	Relative response
Bare	0.157	0.157	1.0
CNS-2	2.0	1.8	22.4
CNS-3	3.0	2.7	109
CNS-5	5.0	4.5	428
CNS-8	8.0	7.2	689
CNS-10	10.0	9.0	661
CNS-12	12.0	10.8	562

The relative neutron fluence responses were normalized to the response of the bare detector in the neutron standard field with a bare ^{241}Am–Be source

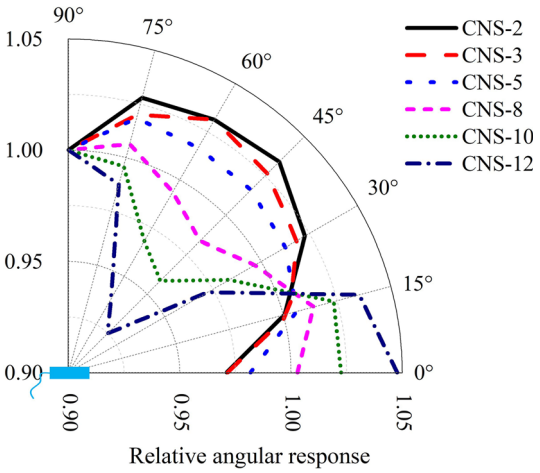

Fig. 2 Simulated relative angular neutron fluence responses of the CNS system as functions of neutron incident angles. The response was normalized to unity at the angle of 90^o

response functions and the IAEA published data revealed good agreements [22]. This means that the MCNP6 simulated data of the CNS system's neutron fluence response functions are reliable.

In the MCNP6 simulations of the CNS neutron fluence response functions, the neutron energy range was varied from 5×10^{-9} to 20 MeV. The neutron cross-sectional library ENDF/B-VIII.0 was used with the thermal neutron cross section taken from "*h-poly.40t*" [27,28]. The fluence response functions of the CNS system were determined as the number of reactions ^{6}Li$(n, t)^4$He occurred within the sensitive volume of the ^{6}LiI(Eu) detector per incident neutron fluence rate unit using the F4 tally and FM4 card of the MCNP6 code. Figure 3 depicts the fluence response functions of the CNS system obtained from the MCNP6 simulations.

2.4 Neutron spectrum unfolding

In the experiments, the two neutron spectrometer systems (i.e., the BSS and the CNS systems) have been irradiated by the same neutron standard fields at the distance of 150 cm from the source for obtaining the count rates (cps) due to the total components of the fields. This distance is typical for performing the calibrations of neutron measuring devices in the neutron fields. The count rate, C_i, of the ith neutron spectrometer is expressed as:

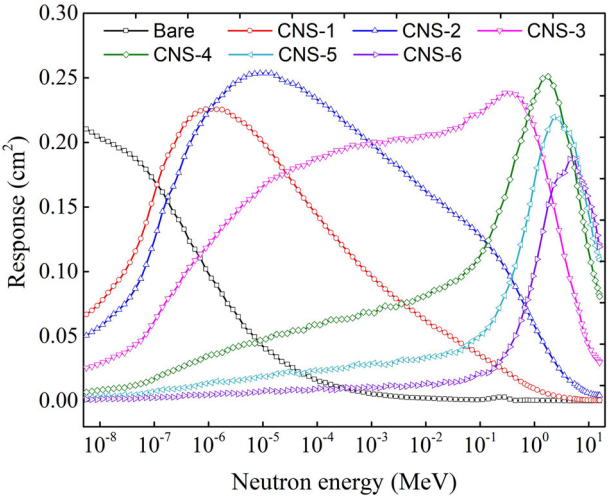

Fig. 3 Simulated neutron fluence response of the CNS system as functions of neutron incident energies

$$C_i = \sum_{b=1}^{\infty} R_{ib}(E_b) \times \varphi_b(E_b) \qquad i = 1, 2, \ldots, 7 \tag{1}$$

where $\varphi_b(E_b)$ is the spectral neutron fluence rate at the energy bin b, E_b. $R_{ib}(E_b)$ is the spectral neutron fluence response function of the ith spectrometer at the neutron energy E_b. In the present work, the response functions, $R_{ib}(E_b)$, of the CNS and the BSS systems were evaluated using the MCNP6 simulations. The $R_{ib}(E_b)$ of the CNS system is depicted in Fig. 3, while that of the BSS system were reported in Ref. [22].

Once the count rates C_i were measured with the CNS and the BSS systems, unfolding processes were performed using the FRUIT code to achieve neutron fluence rate spectra [29], i.e., the spectral neutron fluence rates as functions of neutron energies. The FRUIT code is based on the iterative algorithm of Monte Carlo method to vary the parameters and derive the final spectrum as the conditions of successive spectra fulfilling the established convergence criteria [29]. In order to obtain the neutron fluence rate spectra, the number of energy bins used in the unfolding process was chosen as 115 in the energy range from 5×10^{-9} to 20 MeV, based on 50 energy bins in the same range as reported by the IAEA [26] and the ICRP [30] publications.

As a result of the unfolding process using the FRUIT code, the spectral neutron fluence rate, known as a neutron fluence rate spectrum (expressed as $\mathrm{d}\phi_b/(\mathrm{d}E_b \cdot \mathrm{d}t)$, unit in $\mathrm{cm}^{-2}\,\mathrm{eV}^{-1}\,\mathrm{s}^{-1}$) was determined [31]. The successfully unfolded neutron fluence spectra are acceptable when the deviations between the unfolded and experimental values of all C_i values are less than 3%. Then, the neutron fluence rates ($\varphi_b(E_b) = \mathrm{d}\phi_b/\mathrm{d}t$, unit in $\mathrm{cm}^{-2}\,\mathrm{s}^{-1}$) were calculated as functions of the incident neutron energies.

2.5 Calculations of neutron field parameters

Since a neutron fluence rate spectra are available, the values of φ_E (unit in $cm^{-2}.s^{-1}$) can be calculated as follows [31]:

$$\varphi_E = \sum_{b=1}^{115} \varphi_b(E_b), \tag{2}$$

where $\varphi_b(E_b)$ is the spectral neutron fluence rate in the energy bin b, E_b. The values of $\dot{H}^*(10)$ (unit in μSv/h) are calculated as [31]:

$$\dot{H}^*(10) = \sum_{b=1}^{115} \dot{H}_b(E_b) = \sum_{b=1}^{115} h_\phi(E_b) \times \varphi_b(E_b) \tag{3}$$

where $\dot{H}_b(E_b)$ is the neutron ambient dose equivalent rate in the energy bin b and $h_\phi(E_b)$ is the ICRP 74 fluence-to-ambient dose equivalent conversion coefficient in the energy bin b [30]. Alternatively, the values of $\widetilde{E}$, $\overline{E}$ (unit in MeV) and $\overline{h}_\phi$ (unit in pSv cm^2) can be calculated as follows [31]:

$$\widetilde{E} = \frac{\sum_{b=1}^{115} \dot{H}_b(E_b) \times E_b}{\dot{H}^*(10)}, \tag{4}$$

$$\overline{E} = \frac{\sum_{b=1}^{115} \varphi_b(E_b) \times E_b}{\varphi_E}, \tag{5}$$

and

$$\overline{h}_\phi = \frac{\dot{H}^*(10)}{\varphi_E}. \tag{6}$$

3 Results and discussion

3.1 Neutron fluence rate spectra

Figure 4 shows the neutron fluence rate spectra at the distance of 150 cm from the source, measured by the BSS and the CNS systems in the three neutron standard fields. Figure 4a–c illustrates a good agreement between the neutron fluence rate spectra obtained from the BSS and the CNS systems. This means that the measurements using the CNS system are reliable, and the CNS system can be applied in neutron spectrometry and dosimetry for radiation protection purposes. From Fig. 4d, one can see that the neutron fluence rate spectra measured by the CNS system show a good trend of moderation process. In the neutron standard field of a bare ^{241}Am–Be source, the neutron spectrum has a high fast neutron peak and a low thermal neutron peak. In the moderated fields, the neutron spectra have lower fast neutron peaks and higher thermal neutron peaks. The larger diameter of the spherical moderator of the ^{241}Am–Be source corresponds to a lower fast neutron peak and a higher thermal neutron peak.

3.2 Integrated spectral neutron fluence rate, φ_E

Figure 5 shows the integrated values of φ_E measured by the CNS and the BSS systems. The ratios of the integrated φ_E values obtained from the CNS and the BSS measurements were also calculated as shown in Fig. 5. The standard uncertainties (k=1) of the φ_E values (denoted as u_{φ_E}) are ascribed to be influenced by the factors in Eq. (1). The statistical uncertainties of C_i measurements are affected by the angular responses, which are greater for the CNS system in comparison with the BSS system. The statistical uncertainties of C_i values can be reduced

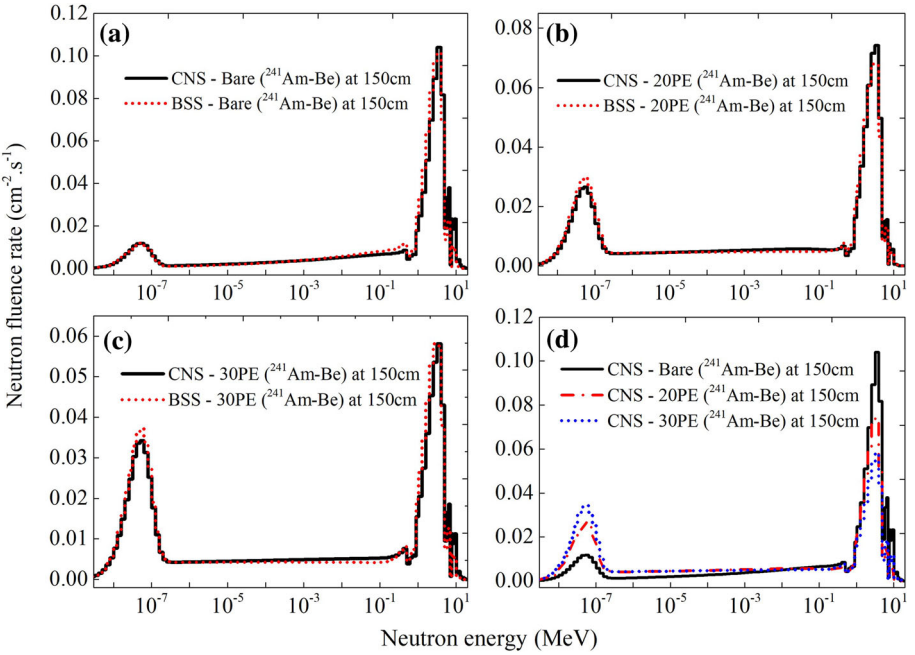

Fig. 4 Neutron fluence rate spectra at the distance of 150 cm from the source in the three neutron standard fields measured by the CNS and the BSS systems

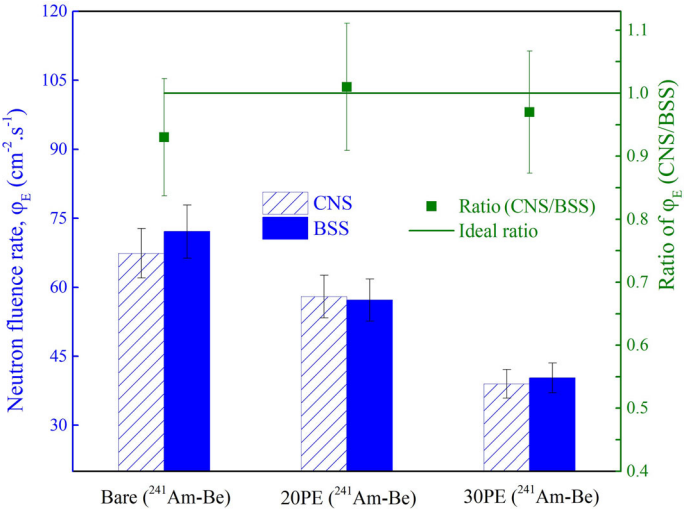

Fig. 5 Integrated neutron fluence rate, φ_E, at the distance of 150 cm from the source in the three neutron standard fields measured by the CNS and the BSS systems. The right vertical axis shows the ratio of φ_E measured by the CNS and the BSS systems. Data were normalized to October 1, 2019

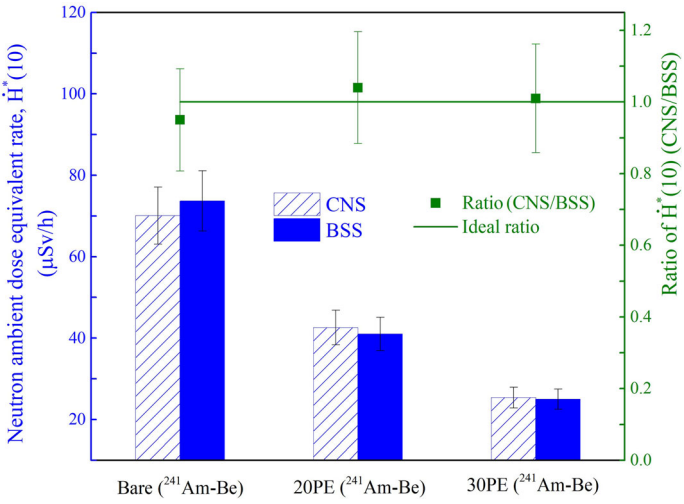

Fig. 6 Integrated neutron ambient dose equivalent rate, $\dot{H}^*(10)$, at the distance of 150 cm from the source in the three neutron standard fields measured by the CNS and the BSS systems. The right vertical axis shows the ratio of $\dot{H}^*(10)$ measured by the CNS and the BSS systems. Data were normalized to October 1, 2019

within 1%. The statistical uncertainties of the simulated $R_{ib}(E_b)$ can also be remained less than 1% by choosing a high number of particle histories. Thus, the u_{φ_E} values are mainly caused by the uncertainties of the unfolding process, which are complicated and influenced by many factors in the unfolding process. These are, however, ascribed to be strongly influenced by the deviations of integrated unfolded and experimental C_i values (about 3% in this work). Therefore, the u_{φ_E} values (k = 1) are estimated of about 7%, which is the same as the largest discrepancy between the values of φ_E determined by the CNS and the BSS measurements in the bare ^{241}Am–Be neutron standard field. The u_{φ_E} values are displayed as vertical bars accompanying with the φ_E values in Fig. 5. The u_{φ_E} values are acceptable and satisfied the ISO criteria in measurements of neutron fluence rate (the acceptable uncertainty of 10% as mentioned in ISO 12789-2:2008 (E) [32]). The standard uncertainties of φ_E ratios are estimated less than 10% and shown as the error bars in Fig. 5.

3.3 Neutron ambient dose equivalent rate, $\dot{H}^*(10)$

Figure 6 shows the integrated values of $\dot{H}^*(10)$ obtained with the CNS system in comparison with that obtained from the BSS measurements. The ratios between the integrated $\dot{H}^*(10)$ values obtained from the CNS and the BSS measurements were also calculated and are presented in Fig. 6. Based on the uncertainty propagation for Eq. 3, the standard uncertainties of the $\dot{H}^*(10)$ (denoted as $u_{\dot{H}^*(10)}$) can be calculated (taking into account the u_{φ_E} values of 7% and the uncertainties of $h_\phi(E_b)$ of 4% [30]). Therefore, the $u_{\dot{H}^*(10)}$ values (k=1) are estimated within 10%. The $u_{\dot{H}^*(10)}$ values are shown as vertical bars accompanying with the $\dot{H}^*(10)$ values in Fig. 6. The standard uncertainties of $\dot{H}^*(10)$ ratios are estimated less than 15% and shown as the error bars in Fig. 6. One can see a good agreement between the $\dot{H}^*(10)$ values obtained from the CNS and the BSS measurements. The largest discrepancy of about 5% is obtained for the measurements in the bare ^{241}Am–Be neutron standard field. This discrepancy is considerably acceptable for radiation protection purpose.

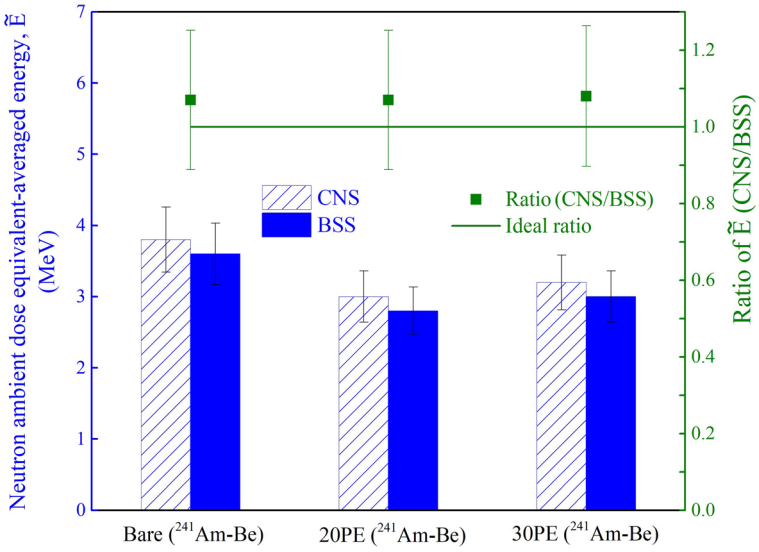

Fig. 7 Neutron ambient dose equivalent-averaged energy, $\widetilde{E}$, at the distance of 150 cm from the source in the three neutron standard fields measured by the CNS and the BSS systems. The right vertical axis shows the ratio of $\widetilde{E}$ measured by the CNS and the BSS systems

3.4 Neutron ambient dose equivalent-averaged energy, $\widetilde{E}$

Figure 7 displays the comparison of the $\widetilde{E}$ values obtained from the CNS and the BSS measurements. The ratios of the $\widetilde{E}$ values obtained from the CNS and the BSS measurements were calculated and are presented in the right vertical axis of Fig. 7. The standard uncertainties of the $\widetilde{E}$ values (denoted as $u_{\widetilde{E}}$) can be calculated based on uncertainty propagation of Eq. 4. The $u_{\dot{H}^*(10)}$ values are about 10%, and the uncertainty of $\dot{H}_b(E_b)$ is ascribed to be less than 4%, similar to the uncertainties of h_ϕ [30]. Therefore, the $u_{\widetilde{E}}$ values are estimated within 12%, which are presented as vertical bars together with the $\widetilde{E}$ values in Fig. 7. The standard uncertainties of $\widetilde{E}$ ratios are estimated less than 17% and shown as the error bars in Fig. 7. The $\widetilde{E}$ values measured by the CNS system are overestimated by about 7–8% compared to that measured by the BSS system. Although the reason of this discrepancy is not clear and needs to be further investigated, it is considerably acceptable for radiation protection purposes. The discrepancy does not lead to the change of $h_\phi(E_b)$, of which the acceptable standard uncertainty (k=1) is 15% as mentioned in ISO 12789-2:2008 (E) [32]).

3.5 Neutron fluence-averaged energy, $\overline{E}$

Figure 8 depicts the values of $\overline{E}$ in comparison between the CNS and the BSS measurements. The ratios of $\overline{E}$ values obtained from the CNS and the BSS were also calculated and are shown in Fig. 8. Similar to the $\widetilde{E}$, the standard uncertainties of the $\overline{E}$ values (denoted as $u_{\overline{E}}$) are estimated within 12% and presented as vertical bars accompanying with the $\overline{E}$ values in Fig. 8. The standard uncertainties of $\overline{E}$ ratios are estimated within 17% as shown in Fig. 8. One can see that the values of $\overline{E}$ obtained from the CNS system are greater than that obtained from the BSS system by about 8–11%. This discrepancy is considerably acceptable for radiation

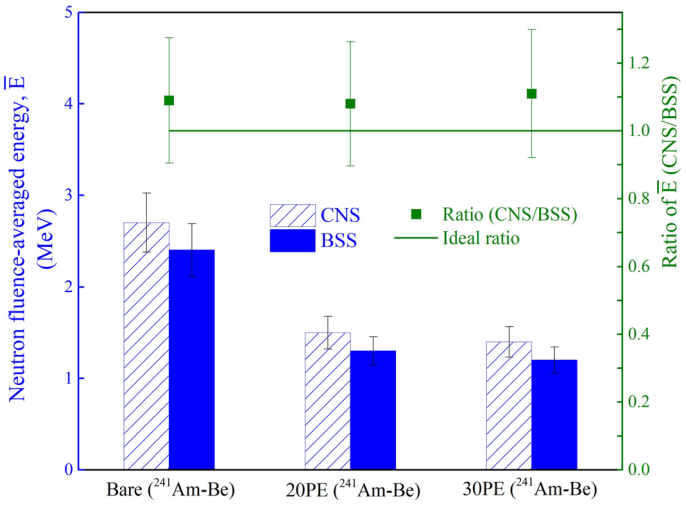

Fig. 8 Neutron fluence-averaged energy, $\overline{E}$, at the distance of 150 cm from the source in the three neutron standard fields measured by the CNS and the BSS systems. The right vertical axis shows the ratio of $\overline{E}$ measured by the CNS and the BSS systems

protection purpose, since this discrepancy does not lead to the change in the values of $h_\phi(E_b)$, whose standard uncertainty of 15% is acceptable as reported in ISO 12789-2:2008 (E) [32]).

3.6 Neutron fluence-to-ambient dose equivalent conversion coefficient, $\overline{h}_\phi$

The values of $\overline{h}_\phi$ were obtained and shown in Fig. 9. The ratios of the $\overline{h}_\phi$ values obtained from the CNS and the BSS measurements were also calculated and are depicted in Fig. 9. The standard uncertainties of the $\overline{h}_\phi$ values (denoted as $u_{\overline{h}_\phi}$) were calculated based on the $u_{\dot{H}^*(10)}$ values (10%) and the u_{φ_E} values (7%). Therefore, the $u_{\overline{h}_\phi}$ values are estimated within 12%. The standard uncertainties of $\overline{h}_\phi$ ratios are within 17% as shown in Fig. 9. One can see that the $\overline{h}_\phi$ obtained from the CNS system are greater than that obtained from the BSS system by about 2–3%. This discrepancy is within the range of $u_{\overline{h}_\phi}$ obtained in this work and is smaller than the acceptable limit of 15% as reported in ISO 12789-2:2008 (E) [32]. This means that the designed CNS system is reliable for neutron safety assessment.

4 Conclusions

A multilayer CNS system for neutron spectrometry and dosimetry has been designed and characterized based on the similar principle of the BSS system. The CNS system consists of the BSS existing ^{6}LiI(Eu) cylindrical thermal neutron scintillator detector (4.0 mm × 4.0 mm) and six cylindrical PE moderators. The optimal dimensions, the angular neutron fluence response and the neutron spectral fluence response functions of the CNS system have been determined using the MCNP6 code. The diameters of six cylindrical PE moderators were selected as 2, 3, 5, 8, 10 and 12 inches (which are same as that of the BSS system). The height-to-diameter ratio of 0.9 was chosen for the six cylindrical PE moderators based on the MCNP6 simulations. The CNS system was then used to measure the dosimetric quantities of

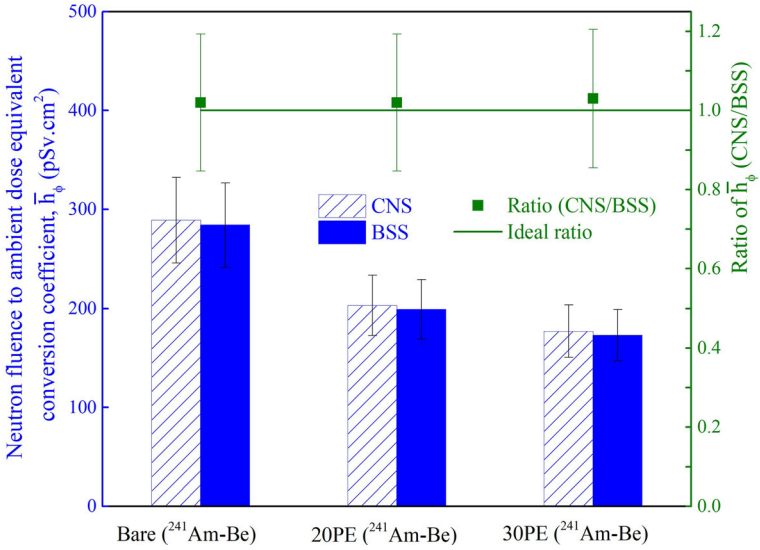

Fig. 9 Neutron fluence-to-ambient dose equivalent conversion coefficients, $\overline{h}_\phi$, at the distance of 150 cm from the source in the three neutron standard fields measured by the CNS and the BSS systems. The right vertical axis shows the ratio of $\overline{h}_\phi$ measured by the CNS and the BSS systems

three neutron standard fields (one of a bare ^{241}Am–Be source and two of moderated ^{241}Am–Be sources) in comparison with that measured by the BSS system. The dosimetric quantities have been evaluated such as integrated spectral neutron fluence rate (φ_E), integrated neutron ambient dose equivalent rate ($\dot{H}^*(10)$), neutron ambient dose equivalent-averaged energy ($\widetilde{E}$), neutron fluence-averaged energy ($\overline{E}$), neutron fluence-to-ambient dose equivalent conversion coefficient ($\overline{h}_\phi$). The standard uncertainties of the dosimetric quantities have been also estimated. The corresponding standard uncertainties (k=1) were obtained as $u_{\varphi_E} = 7\%$, $u_{\dot{H}^*(10)} = 10\%$, $u_{\widetilde{E}} = 12\%$, $u_{\overline{E}} = 12\%$ and $u_{\overline{h}_\phi} = 12\%$, respectively. The discrepancies of the dosimetric quantities measured by the CNS and the BSS systems are 7%, 5%, 8%, 11% and 3%, respectively. The discrepancies falls within the range of the corresponding standard uncertainties of the dosimetric quantities and are considerably acceptable for radiation protection purposes. The results indicate that the designed CNS system is qualified for neutron spectrometry and dosimetry. The advantage of the CNS system is due to its compactness, portability and simplicity in fabrication.

Acknowledgements This research was funded by the Ministry of Science and Technology, Vietnam, through the supervision of Vietnam Atomic Energy Institute under Grant 08/HĐ/ĐTCB. The authors would like to thank Dr. Do Duc Nguyen and Dr. Trieu Viet Phuong of the Vietnam Metrology Institute and Ms. Dang Thi My Linh of the Institute for Nuclear Science and Technology for their kind help. Dr. Le Bao Trung of the North Dakota State University (ND, USA) is highly appreciated for his kind proofreading of the manuscript.

Data Availability Statement This manuscript has associated data in a data repository [Authors' comment: Data will be available from the corresponding authors upon request.]

Declarations

Conflict of interest The authors declare that they have no conflict of interest regarding the publication of this paper.

References

1. J.A. Cruzate, J.L. Carelli, B.N. Gregori, in *12th Congress of the International Radiation Protection Association (IRPA12)*. 19–24 October, 2008. Buenos Aires, Argentina. Bonner Sphere Spectrometer: A CONRAD Project Intercomparison (2008). https://www.foroiberam.org/documents/193375/199940. Accessed 19 Mar 2021
2. D.J. Thomas, A.V. Alevra, Bonner sphere spectrometers—critical review. Nucl. Instrum. Methods Phys. Res. A **476**, 12–20 (2002). https://doi.org/10.1016/S0168-9002(01)01379-1
3. T.N. Le, H.N. Tran, K.T. Nguyen, G.V. Trinh, Neutron calibration field of a bare ^{252}Cf source in Vietnam. Nucl. Eng. Technol. **49**, 277–284 (2017). https://doi.org/10.1016/j.net.2016.07.011
4. T.N. Le, H.N. Tran, Q.N. Nguyen, G.V. Trinh, K.T. Nguyen, Characterization of a neutron calibration field with ^{241}Am–Be source using Bonner sphere spectrometers. Appl. Radiat. Isot. **133**, 68–74 (2018). https://doi.org/10.1016/j.apradiso.2017.12.012
5. T.N. Le, S.M.T. Hoang, Q.N. Nguyen, L. Thiansin, H.N. Tran, Simulated workplace neutron fields of ^{241}Am–Be source moderated by polyethylene spheres. J Radioanal. Nucl. Chem. **321**, 313–321 (2019). https://doi.org/10.1007/s10967-019-06577-8
6. T.N. Le, H.N. Tran, T.D. Duong, Q.N. Nguyen, T.Q. Ho, G.V. Trinh, K.T. Nguyen, Evaluation of gamma contribution in a neutron calibration field of ^{241}Am–Be source. Appl. Radiat. Isot. **133**, 117–120 (2018). https://doi.org/10.1016/j.apradiso.2018.01.001
7. J. Dubeau, S.S. Hakmana Witharana, J. Atanackovic, A. Yonkeu, J.P. Archambault, A neutron spectrometer using nested moderators. Radiat. Prot. Dosim. **150**(2), 217–222 (2012). https://doi.org/10.1093/rpd/ncr381
8. R. Maglieri, A. Licea, M. Evans, J. Seuntjens, J. Kilde, Measuring neutron spectra in radiotherapy using the nested neutron spectrometer. Med. Phys. **42**(11), 6162–6169 (2015). https://doi.org/10.1118/1.4931963
9. J. Atanackovic, W. Matysiak, S.S. Hakmana Witharana, I. Aslam, J. Dubeau, A.J. Waker, Neutron spectrometry and dosimetry study at two research nuclear reactors using Bonner sphere spectrometer (BSS), rotational spectrometer (ROSPEC) and cylindrical nested neutron spectrometer (NNS). Radiat. Prot. Dosim. **154**(3), 364–374 (2012). https://doi.org/10.1093/rpd/ncs248
10. N. Ghal-Eh, M. Kalaei, A. Mohammadi, H.R. Vega-Carrillo, Replacement of Bonner spheres with polyethylene cylinders for the unfolding of an ^{241}Am–Be neutron energy spectrum. Appl. Rad. Isot. **128**, 292–296 (2017). https://doi.org/10.1016/j.apradiso.2017.07.043
11. T. Liamsuwan, J. Channuie, S. Wonglee, M. Kowatari, S. Nishino, Characterization of an in-house developed multi-cylindrical moderators neutron spectrometer. Radiat. Prot. Dosim. **180**(1–4), 94–97 (2018). https://doi.org/10.1093/rpd/ncx215
12. Z. Wang, R.M. Howell, S.F. Kry, E.A. Burgett, N.E. Hertel, M. Salehpour, Characterization of an gold-and-indium dual activation foil-based Bonner sphere system. Nucl. Technol. **168**(3), 603–609 (2009). (**10.13182/NT09-A9276**)
13. E. Aza, N. Dinar, G.P. Manessi, M. Silari, A Bonner sphere spectrometer for pulsed fields. Radiat. Prot. Dosim. **168**(2), 149–153 (2016). https://doi.org/10.1093/rpd/ncv180
14. H.R. Vega-Carrillo, E. Manzanares-Acuña, Background neutron spectrum at 2420 m above sea level. Nucl. Instrum. Methods Phys. Res. A **524**, 146–151 (2004). https://doi.org/10.1016/j.nima.2004.01.044
15. H. Park, J. Kim, K.O. Choi, Neutron calibration facility with radioactive neutron sources at KRISS. Radiat. Prot. Dosim. **126**, 159–162 (2007). https://doi.org/10.1093/rpd/ncm034
16. R. Bedogni, C. Domingo, N. Roberts, D.J. Thomas, M. Chiti, A. Esposito, M.J. Garcia, A. Gentile, Z.Z. Liu, M. De-San-Pedro, Investigation of the neutron spectrum of americium-beryllium sources by Bonner sphere spectrometry. Nucl. Instrum. Methods Phys. Res. A **763**, 547–562 (2014). https://doi.org/10.1016/j.nima.2014.06.040
17. H.R. Vega-Carrillo, E. Gallego, A. Lorente, P.R. Isabel, R. Méndez, Neutron features at the UPM neutronics hall. Appl. Radiat. Isot. **70**, 1603–1607 (2012). https://doi.org/10.1016/j.apradiso.2012.05.003
18. R. Bedogni, D. Bortot, B. Buonomo, A. Esposito, J.M. Gömez-Ros, M.V. Introini, G. Mazzitelli, M. Moraleda, A. Pola, A.M. Romero, A single-exposure, multidetector neutron spectrometer for workplace monitoring. Radiat. Prot. Dosim. **170**, 326–330 (2016). https://doi.org/10.1093/rpd/ncv380
19. J.M. Gómez-Ros, R. Bedogni, D. Bortot, C. Domingo, A. Esposito, M. Introini, M. Lorenzoli, G. Mazzitelli, M. Moraleda, A. Pola, D. Sacco, Two new single-exposure, multi-detector neutron spectrometers for radiation protection applications in workplace monitoring. Radiat. Prot. Dosim. **173**, 104–110 (2017). https://doi.org/10.1093/rpd/ncw349
20. C.J. Werner (ed.), *MCNP User's Manual, Code Version 6.2* (Los Alamos National Laboratory, USA, 2017)
21. R.J. McConn Jr, C.J. Gesh, R.T. Pagh, R.A. Rucker, R.G. Williams III, Compendium of material composition data for radiation transport modeling (PNNL-15870 Rev 1). Pacific North West National Labora-

tory, Richland, WA. USA. (2011). https://www.pnnl.gov/main/publications/external/technical_reports/PNNL-15870Rev1.pdf. Accessed 19 Mar 2021
22. T.N. Le, Establishment of neutron reference fields in Vietnam: a review. Philipp. J. Sci. **149**(3–a), 947–954 (2020)
23. Ludlum Measurements. Inc, *Ludlum Model 42-41 & 42-41L, "Prescila" neutron probe*. https://ludlums.com/images/product_manuals/M42-41_&_M42-41L.pdf. Accessed 19 Mar 2021)
24. M. Maciak, N. Golnik, K. Dworecki, S. Domański, P. Tulik, A. Araszkiewicz, Passive multi-layer neutron spectrometer for neutron radiation dosimetry, in *Proceedings Volume 9662, Photonics Applications in Astronomy, Communications, Industry, and High-Energy Physics Experiments* (2015). https://doi.org/10.1117/12.2202441
25. IEC 61005:2014-07 (Edition 3.0), Radiation protection instrumentation—neutron ambient dose equivalent (rate) meter, in *International Electrotechnical Commission, Geneva 20, Switzerland* (2014)
26. IAEA Technical Reports Series No.403. Compendium of neutron spectra and detector responses for radiation protection purposes—supplement to technical reports series No. 318. IAEA, Technical Report, 2001. https://www-pub.iaea.org/MTCD/Publications/PDF/TRS403_scr.pdf. Accessed 19 Mar 2021
27. J.L. Conlin, W. Haeck, D. Neudecker, D.K. Parsons, M.C. White, Release of ENDF/B-VIII.0-based ACE data files. Technical Report (2018). https://mcnp.lanl.gov/pdf_files/la-ur-18-24034.pdf. Accessed 19 Mar 2021
28. D.K. Parsons, C.A. Toccoli, Re-release of the ENDF/B VIII.0 S(α,β) data processed by NJOY2016. Technical Report, (2020). https://doi.org/10.2172/1634930
29. R. Bedogni, C. Domingo, A. Esposito, F. Fernandez, FRUIT: an operational tool for multisphere neutron spectrometry in workplaces. Nucl. Instrum. Methods Phys. Res. A **580**, 1301–1309 (2007). https://doi.org/10.1016/j.nima.2007.07.033
30. ICRP Publication 74, Conversion coefficients for use in radiological protection against external radiation. Annals of the ICRP 26, 3-4, Technical Report, (1996)
31. ISO 8529-1:2001 (E), Reference neutron radiations—part 1: characteristics and methods of production. International Standard Organization, Switzerland, Technical Report, p. 32 (2001)
32. ISO 12789-2:2008 (E), Reference radiation fields—simulated workplace neutron fields—part 2: calibration fundamentals related to the basic quantities. International Standard Organization, Switzerland, Technical Report, p. 22 (2008)